Biomaterials Science

ROYAL SOCIETY OF CHEMISTRY

PAPER

View Article Online
View Journal | View Issue

Cite this: *Biomater. Sci.*, 2025, **13**, 210

Photoinitiator-free light-mediated crosslinking of dynamic polymer and pristine protein networks†

Riccardo Rizzo, *[a,b] Dylan M. Barber, [b] Jackson K. Wilt, [b] Alexander J. Ainscough [a,b] and Jennifer A. Lewis *[a,b]

Received 25th June 2024,
Accepted 14th October 2024

DOI: 10.1039/d4bm00849a

rsc.li/biomaterials-science

Light-based patterning of synthetic and biological hydrogels enables precise spatial and temporal control over the formation of chemical bonds. However, photoinitiators are typically used to generate free radicals, which are detrimental to human cells. Here, we report a photoinitiator- and radical-free method based on *ortho*-nitrobenzyl alcohol (*o*NBA) photolysis, which gives rise to highly reactive nitroso and benzaldehyde groups. Synthetic hydrogel and pristine protein networks can rapidly form in the presence of these photo-generated reactive species. Thiol -*o*NBA bonds yield dynamic hydrogel networks (DHNs) *via* *N*-semimercaptal linkages that exhibit thixotropy, stress relaxation, and on-demand reversible gel-to-liquid transitions, while amine-*o*NBA bonds can be exploited to crosslink pristine proteins, such as gelatin and fibrinogen, by targeting their primary amines. Since this approach does not require incorporation of photoreactive moieties along the backbone, the resulting crosslinked proteins are well suited for bioadhesives. Our photoinitiator-free platform provides a versatile approach for rapidly creating synthetic and biological hydrogels for applications ranging from tissue engineering to biomedical devices.

Introduction

Light offers contactless, high-precision spatiotemporal control over the biochemical and biophysical properties of hydrogels.[1–10] Yet, most systems require photoinitiators to trigger crosslinking *via* free-radical formation. When such processes occur in the presence of human cells, reactive oxygen species (ROS) are generated that induce cellular oxidative stress and damage DNA, proteins, and lipids.[11–16] As recently shown, the development of photoinitiator- and radical-free crosslinking methods reduces cytotoxicity and improves print resolution.[11] Nevertheless, (meth)acryloyl photoresins remain ubiquitous due to their ease of use and commercial availability. However, they form heterogeneous, brittle networks that contain hydrophobic kinetic chains and potentially toxic unreacted groups.[17–19] Emerging efforts based on step-growth crosslinking *via* photo-click chemistry produce homogeneous hydrogels under mild conditions with improved kinetics and mechanical properties.[20,21] Unfortunately, both approaches incorporate radical-generating photoinitiators making them less suitable for tissue engineering and biomedical devices.

Photoresins that combine the benefits of step-growth with photoinitiator- and radical-free chemistries offer a promising alternative. To facilitate adoption, they must be readily synthesized and offer performance advantages over existing hydrogel chemistries. For example, there would be considerable interest in the photogeneration of dynamic hydrogel networks (DHNs), that exhibit stress-relaxing properties and better recapitulate the nature and dynamics of the native extracellular matrix (ECM).[22–25] The ability to directly create hydrogel networks from pristine proteins would obviate the need to incorporate photoreactive groups. To realize this potential, we posit that both synthetic and biological hydrogels can be realized using nitrobenzyl photochemistry.

Nitrobenzyl derivatives represent one of the most studied photoactive groups due to their ease of synthesis and rapid photolysis.[26] While primarily used as photolabile groups to construct photodegradable materials for biological applications, there is renewed interest in *ortho*-nitrobenzyl derivatives as reactive sites for photocrosslinking of polymer networks.[27] For example, the photolysis-induced formation of benzaldehyde and nitroso groups from *o*-nitrobenzyl alcohols (*o*NBA) has been investigated for reaction with hydrazines (forming hydrazones),[28] and amines (forming imines).[29–32] Moreover, a recent study revealed that an *o*NBA handle with an electron-withdrawing amide group displays excellent reactivity

[a]*Wyss Institute for Biologically Inspired Engineering, Harvard University, Boston, MA 02115, USA. E-mail: jalewis@seas.harvard.edu, rrizzo@seas.harvard.edu*
[b]*Harvard John A. Paulson School of Engineering and Applied Sciences, Harvard University, Cambridge, MA 02138, USA*

† Electronic supplementary information (ESI) available. See DOI: https://doi.org/10.1039/d4bm00849a

towards primary amines (PANAC reaction) to form indazolone heterocycles.[33]

Here, we demonstrate that a single amide *o*NBA handle can be used for photoinitiator-free, step-growth crosslinking of thiolated polymers forming DHNs and of pristine proteins containing primary amines (Fig. 1A-I). We investigated the photoreactivity of the *o*NBA handle and compared *o*NBA-based hydrogel resins to those based on photoinitiators. We explored the crosslinking performance and tunability of thiol-*o*NBA and amine-*o*NBA PEG-based photoresins *via* photorheology as a function of pH, concentration, and light intensity. We then confirmed the biocompatibility of these photocrosslinking mechanisms in the presence of human fibroblasts as well as carried out feasibility experiments focused on 3D printing and bioadhesion. Our photoinitiator-free platform provides a versatile approach for rapidly creating synthetic and biological hydrogels for applications ranging from tissue engineering to biomedical devices.

Experimental

*o*NBA and m-*o*NBA synthesis

The synthesis procedure was adapted from Guo *et al.*[33] In short, 5 g (19.2 mmol) of 4-bromomethyl-3-nitrobenzoic acid and 9.3 g (67.3 mmol) of potassium carbonate were dissolved in 150 mL of 1 : 1 water : acetone solution and refluxed at 60 °C for 3 h. Acetone was removed under vacuum and the aqueous phase was extracted twice with diethyl ether. The aqueous phase was acidified with the addition of 1 M HCl until pH ≤ 1, and then extracted twice with ethyl acetate. The combined organic phases were washed with water and brine, dried over magnesium sulfate (MgSO4), filtered and concentrated in vacuum without further purification to afford 4-(hydroxymethyl)-3-nitrobenzoic acid (*o*NBA) as a brown-orange solid (3.44 g, 90%). Identity of the compound was verified by ^{1}H-NMR (see ESI, Fig. S1 and 2†).

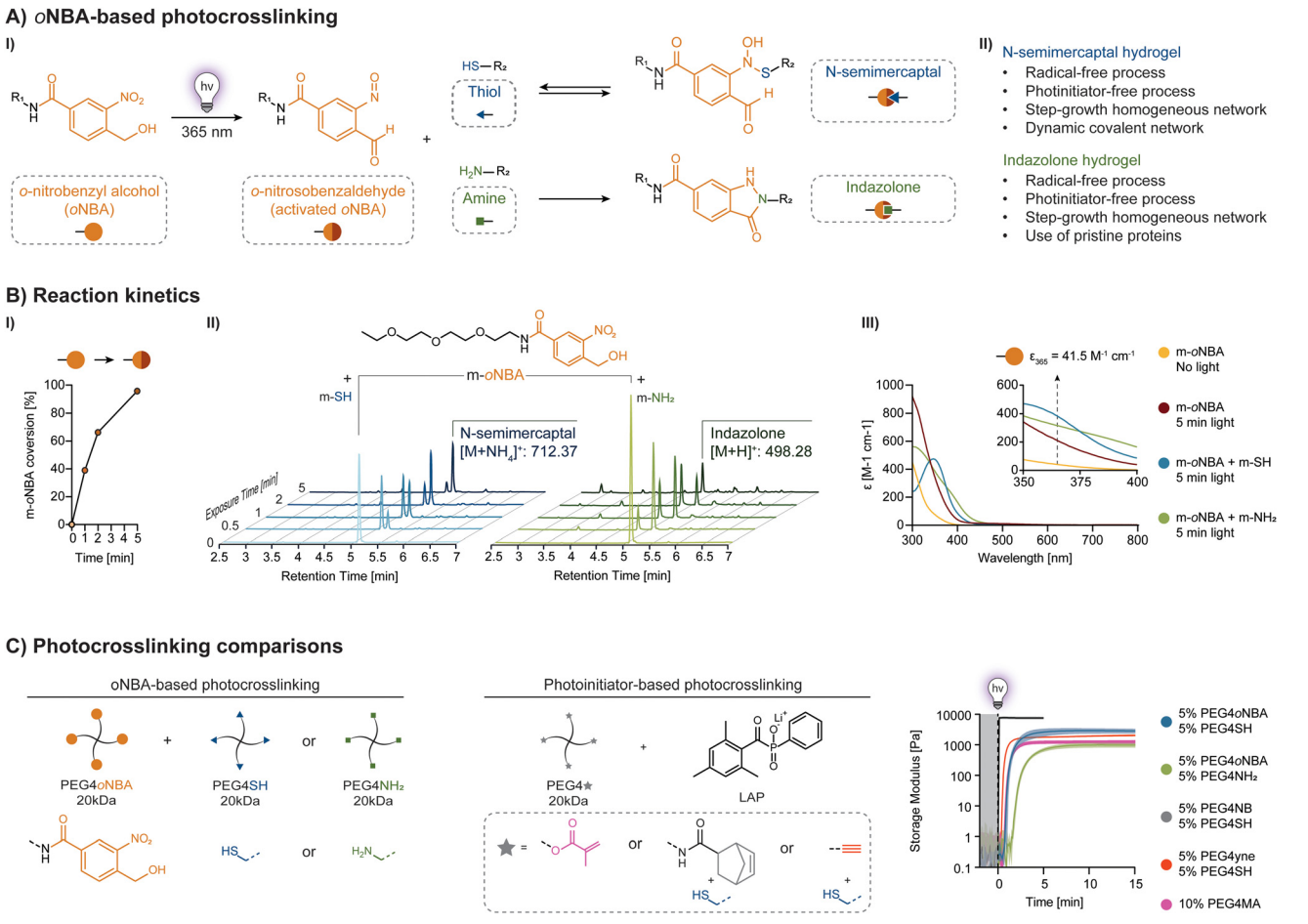

Fig. 1 (A) Schematics of *ortho*-nitrobenzyl alcohol (*o*NBA)-based photocrosslinking reaction mechanisms. Upon absorption of UV light (365 nm), *o*NBA photolysis leads to an activated form with benzaldehyde and nitroso groups. A thiol nucleophilic addition to the nitroso residue results in the formation of a *N*-semimercaptal dynamic bond. An amine nucleophilic addition to the nitroso or benzaldehyde group leads instead to the formation of an indazolone bond (I). Both mechanisms arise from the photoreactive moiety (*o*NBA) and proceed under mild, photoinitiator- and radical-free conditions, leading to the generation of step-growth dynamic hydrogel networks (DHNs) for the *N*-semimercaptal bond or step-growth networks with pristine proteins for the indazolone bond (II). (B) Reaction kinetics (I and II) and absorption spectra (III) using small monofunctional molecules (m-*o*NBA, m-SH, and m-NH_2). (C) Comparison of photocrosslinking performance of thiol-*o*NBA (blue) and amine-*o*NBA (green) chemistries with the known photoinitiator-based chemistries: thiol–norbornene (grey), thiol–yne (red), and methacrylate (pink) that use LAP as photoinitiator.

250 mg (1.27 mmol, 1 eq.) of 4-(hydroxymethyl)-3-nitrobenzoic acid (*o*NBA) was dissolved in 5 mL of dichloromethane in the presence of 500 mg (3.22 mmol, ~2.5 eq.) of *N*-(3-dimethylaminopropyl)-*N*′-ethylcarbodiimide hydrochloride (EDC) and 225 mg (1.95 mmol, ~1.5 eq.) of *N*-hydroxysuccinimide (NHS). The reaction was stirred for 15 min at room temperature. 960 μL (5.3 mmol, ~4 eq.) of 2-(2-(2-ethoxyethoxy)ethoxy)ethanamine and 10 μL of *N*,*N*-diisopropylethylamine were then added dropwise to the stirring reaction mixture. The reaction was left to proceed for 6 h and the product was then purified by flash chromatography (dichloromethane : methanol 95 : 5, R_f: 0.2). Identity of the compound was verified by LC-MS (*m*/*z*: [M + H] calcd 357.16, found 357.16) and ^{1}H-NMR (see ESI, Fig. S3 and 4†).

PEG4*o*NBA synthesis

*o*NBA terminated four-arm PEG was synthesized by dissolving 200 mg (1 mmol, 20 eq.) of 4-(hydroxymethyl)-3-nitrobenzoic acid (*o*NBA) in 5 mL of dimethylsulfoxide in the presence of 390 mg (2 mmol, 20 eq.) of *N*-(3-dimethylaminopropyl)-*N*′-ethylcarbodiimide hydrochloride (EDC) and 230 mg (2 mmol, 20 eq.) of *N*-hydroxysuccinimide (NHS). The reaction was stirred for 30 min at room temperature. A solution of 250 mg (0.05 mmol of NH_2, 1 eq.) PEG4NH_2 (20 kDa) in 2 mL H_2O with 10 μL of *N*,*N*-diisopropylethylamine was then added dropwise. As the reaction becomes turbid within 1 h, addition of a minimum amount (~2 mL) of acetonitrile was necessary to maintain a clear solution. The reaction was left to proceed for 18 h, and dialyzed against 5 : 3 acetonitrile : water (SpectraPor® Biotech RC, MWCO: 3.5–5 kDa) for 4 days. The solution was then centrifuged at 4000 rpm for 5 min to eliminate precipitates. Acetonitrile was removed from supernatant under vacuum and remaining PEG4*o*NBA suspension was freeze-dried. Lyophilized PEG4*o*NBA was stored under inert atmosphere at −20 °C prior to use. Identity of the compound was verified *via* ^{1}H-NMR (see ESI, Fig. S5†).

HA synthesis

Three types of photoactive hyaluronic acid were synthesized: (1) thiolated-hyaluronic acid (HA-SH), (2) methacrylated hyaluronic acid (HA-MA), and (3) *o*NBA modified hyaluronic acid (HA-*o*NBA). HA-SH was synthesized by dissolving 350 mg (0.87 mmol, 1 eq.) of HA (250 or 100 kDa, HTL Biotechnology) overnight, while stirring, in 140 mL of 150 mM MES buffer pH 4.5. Next, 21 mg (0.176 mmol SH, ~0.2 eq.) of 3,3′-dithiobis (propionohydrazide) (DTPHY) and 67.9 mg (0.44 mmol, ~0.5 eq.) of *N*-(3-dimethylaminopropyl)-*N*′-ethylcarbodiimide hydrochloride (EDC), pre-dissolved in minimum amount of water, were added dropwise to the stirring solution and the reaction was left to proceed overnight (18 h). Disulfide bridges were reduced with 150 mg (0.6 mmol, ~0.7 eq.) of tris(2-carboxyethyl)phosphine hydrochloride (TCEP) pre-dissolved in a minimum amount of MES buffer. The reaction mixture was left under gentle stirring overnight in a sealed flask. After addition of 1 g of sodium chloride (NaCl), the solution was dialyzed (ThermoFisher SnakeSkin™, MWCO: 3.5 kDa) against acidified mQ H_2O (pH 4 using HCl) for 5 days with frequent water changes and freeze-dried. Lyophilized HA-SH was stored under inert atmosphere at −20 °C prior to use. The degree of substitution (DS) was estimated to be ~0.25 mmol of SH per gram of HA (~10% of disaccharide units) with ^{1}H-NMR in D_2O using internal standard 3-(trimethylsilyl)-1-propanesulfonic acid (DSS, 2H, ~0.75 ppm) and hydrazide methylene protons (~2.7 and 2.8 ppm, see ESI, Fig. S6†).

HA-MA was synthesized by dissolving 100 mg (0.25 mmol, 1 eq.) of HA (250 kDa, HTL Biotechnology) overnight, while stirring, in 10 mL of PBS pH 7.4. 372 μL (0.25 mmol, 1 eq.) of methacrylic anhydride was then added dropwise to the stirring solution. The pH was monitored after 10 min, 30 min, 2 h and 6 h and a 2 M sodium hydroxide (NaOH) solution was used to restore a neutral pH 7. The reaction was left to proceed for additional 18 h, after which pH was adjusted to 7, and 1 g of NaCl was added and left to dissolve. The solution was then centrifuged at 4000 rpm for 3 min to spin down the excess of acrylic acid, supernatant was dialyzed (MWCO: 3.5 kDa) against milliQ water for 5 days with frequent water changes and freeze-dried. Lyophilized HA-MA was stored under inert atmosphere at −20 °C prior to use. The degree of substitution (DS) was estimated to be ~0.23 mmol of MA per gram of HA (~9% of disaccharide units) with ^{1}H-NMR in D_2O using internal standard 3-(trimethylsilyl)-1-propanesulfonic acid (DSS, 2H, ~0.75 ppm) and methacrylate protons (~6.1 and 6.2 ppm, see ESI, Fig. S7†).

HA-*o*NBA was synthesized by dissolving 75 mg (0.38 mmol, 1 eq.) of 4-(hydroxymethyl)-3-nitrobenzoic acid (*o*NBA) in 2 mL of dimethylsiloxane (DMSO) in the presence of 146 mg (0.94 mmol, ~2.5 eq.) of *N*-(3-dimethylaminopropyl)-*N*′-ethylcarbodiimide hydrochloride (EDC) and 86 mg (0.74 mmol, ~2 eq.) of *N*-hydroxysuccinimide (NHS). The reaction was monitored by HPLC and completed (no residual *o*NBA peak) after 30 min at room temperature. 42 mg (0.25 mmol, ~0.7 eq.) of 2-aminoethyl methacrylate hydrochloride (MA-NH_2). The reaction was left to proceed for 7 h until ~70% consumption of *o*NBA-NHS (monitored by HPLC, see ESI Fig. S8†) to form *o*NBA-*N*-MA, and then added dropwise to a stirring solution of 0.25% HA-SH (250 or 100 kDa, DS: 10%) in 70 mL PBS pH 7.4. The reaction was left to proceed for 18 h and then dialyzed (MWCO: 3.5 kDa) against milliQ water for 5 days with frequent water changes and freeze-dried. Lyophilized HA-*o*NBA was stored under inert atmosphere at −20 °C prior to use. The successful grafting of *o*NBA moieties was confirmed with ^{1}H-NMR (see ESI, Fig. S9†).

fGel-SH synthesis

Thiolated fish gelatin (fGel-SH) was synthesized based on the protocol from Rizzo *et al.*[34] Briefly, 0.5 g of fish gelatin (gelatin from cold water fish skin, Sigma-Aldrich) was dissolved in 25 mL 150 mM MES buffer pH 4.5. Next, 48 mg of DTPHY and 80 mg of EDC were added to the reaction solution under stirring and the reaction was left to proceed for 24 h. 287 mg of TCEP was then added, and the reduction of disulfides was left to proceed for 8 h under gentle stirring. After addition of 0.5 g

of sodium chloride (NaCl), the solution was dialyzed (ThermoFisher SnakeSkin™, MWCO: 3.5 kDa) against acidified mQ H_2O (pH 4 using HCl) for 5 days with frequent water changes and freeze-dried. Lyophilized fGel-SH was stored under inert atmosphere at −20 °C prior to use. The degree of substitution (DS) was estimated to be ~0.34 mmol of SH per gram of fGel with ^{1}H-NMR in D_2O using internal standard 3-(trimethylsilyl)-1-propanesulfonic acid (DSS, 2H, ~0.75 ppm) and hydrazide methylene protons (~2.7 and 2.8 ppm, see ESI, Fig. S10†).

Reaction kinetics and absorption spectra

NMR spectra were acquired on a Bruker AVANCE NEO 400. High performance liquid chromatography (HPLC) was performed using an Agilent 1260 Infinity II system, equipped with a Poroshell 120 EC-C18 4.6 × 100 mm, 2.7 μm particle size column using a gradient from 5 to 95% acetonitrile (ACN) in water over 9 min at 1 mL min^{-1}. Liquid chromatography-mass spectroscopy (LC-MS) was performed on a Bruker MicroTof MS equipped with electrospray ionization (ESI). Amide monofunctional *o*NBA (m-*o*NBA), *O*-(2-mercaptoethyl)-*O*′-methyl-hexa(ethylene glycol) (m-SH) and 2-(2-(2-ethoxyethoxy)ethoxy)ethanamine (m-NH_2) were dissolved in water at 20 mM. Solutions were mixed to obtain the formulations used for Fig. 1B (10 mM m-*o*NBA + 10 mM m-SH, 10 mM m-*o*NBA + 10 mM m-NH_2, and 10 mM m-*o*NBA). Using a 20 mm geometry and the same light setup adopted for photorheology (365 nm UV light at 20 mW cm^{-2}), 16 μL of the various solutions were irradiated for 0, 0.5, 1, 2 and 5 min. The solutions were diluted 1 : 100 in water for HPLC analysis or diluted 1 : 500 for LC-MS analysis (m-*o*NBA solution). Using the non-exposed samples as controls, the consumption of m-*o*NBA was calculated by measuring its peaks integral. For the absorption spectra, 2 μL of each (undiluted) solution were analyzed at 25 °C, with 1 nm step, using a BioTek Synergy HT reader equipped with Take3 microplate, and subtracting water background. For NMR (ESI, Fig. S11–S14†), 0.5 mL of solutions in D_2O were irradiated for 15 min in a glass vial (365 nm UV light at 20 mW cm^{-2}) prior to measurement.

Photorheology

Photorheology was carried out on a Discovery HR 20 (TA instruments) rheometer equipped with an 8 mm parallel plate stainless steel geometry and quartz glass floor. Omnicure Series2000 lamp (Lumen Dynamics) with 365 nm bandpass filter was used as light source. Light intensity at the sample location was measured with PMA2100 (Solar Light) radiometer meter with PMA2107 UVA + B sensor. The various polymers (10–20% PEGs, 2–5% HA, 10–20% fGel), and 2% LAP stock solutions were prepared in PBS (pH 7.4, unless otherwise indicated), and PEG4*o*NBA stock solution was prepared at 20% in DMSO. The photoresins were prepared by mixing and diluting in PBS the stock solutions to obtain the desired final concentration of the various components. Oscillatory measurements were performed in triplicate, at room temperature, using 3 μL of photoresin in 50 μm gap, at 1 Hz frequency and 1% shear rate and ~6.8 s point duration. The tests were carried out in the dark and in the presence of a water-soaked tissue to prevent the sample from drying. For each measurement, light irradiation (365 nm, 10–30 mW cm^{-2}) was initiated after 120 s. End point storage and loss moduli were reported, and the minimum light exposure needed to reach 30% of final storage modulus was used to assess crosslinking kinetics. To facilitate comparison between different chemistries, the PEG-based photoresins contained the same polymer concentration, polymer molecular weight, and functionality.

Shear thinning behavior of 1.3% PEG4*o*NBA/1% HA-SH (250 kDa, DS: 10%) was characterized by stress viscometry. Photoresin (3 μL) was first crosslinked as previously indicated (50 μm gap, 15 min light exposure, 365 nm, 20 mW cm^{-2}). A logarithmic sweep was then performed as a function of increasing shear rate from 0.1 s^{-1} to 1000 s^{-1} (10 points measured per decade). Next, the shear recovery behavior was determined after photoresin crosslinking (50 μm gap, 15 min light exposure, 365 nm, 20 mW cm^{-2}) using oscillatory measurements with varying shear strain at a constant frequency of 1 Hz. In the first interval (resting), a shear strain of 1% was applied for 120 s. In the second interval, a 600% shear strain was applied for 60 s, followed by a 5 s interval at 1% strain to allow the material to rest and a 240 s interval at the same strain (recovery). The same cycle was then repeated resulting in a resting-high shear recovery-resting-high shear recovery sequence. Their gel-to-liquid (dissolution) behavior was assessed (Fig. 3VI) by carrying out oscillatory measurements at 1% strain and 1 Hz frequency. After crosslinking the photoresin (50 μm gap, 15 min exposure to light; 365 nm, 20 mW cm^{-2}), a solution of 1 M *O*-(2-mercaptoethyl)-*O*′-methyl-hexa(ethylene glycol) (m-SH) in PBS was gently pipetted around the geometry. Their storage modulus was measured for 2.5 h. The 2.5% HA-*o*NBA/10% fGel storage modulus was measured by a similar procedure, with a solution of 1 M Glycine or PBS pipetted around the geometry upon crosslinking (5 min irradiation). For the dissolution data shown in Fig. 3VI, hydrogels were prepared as previously described, incubated in diluted Rhodamine-maleimide PBS solution for 24 h, washed 3× in PBS, and then incubated for 3 h in either PBS (control) or 1 M *O*-(2-mercaptoethyl)-*O*′-methyl-hexa(ethylene glycol) (m-SH) in PBS. Optical images of these samples were taken at 0, 1 and 3 h.

Stress relaxation

Hydrogels composed of 1.3% PEG4*o*NBA/1% HA-SH (250 kDa, DS: 10%) were prepared by casting the photoresin in PDMS rings (4 mm diameter, 1.5 mm height) and exposing them for 15 min to a 365 nm light with 20 mW cm^{-2} intensity. They were then removed from the PDMS molds and equilibrated in PBS for 24 h. Discovery HR 20 (TA instruments) equipped with an 8 mm stainless steel flat geometry was used to carry out stress relaxation tests. Samples were placed between the plates and compression to 30% strain was performed at 20 μm s^{-1}. Samples were held under constant strain for 1 h, while the variation in axial stress was measured.

Swelling

The photoresins 1.3% PEG4*o*NBA/1% HA-SH (250 kDa, DS: 10%) and 2.5% HA-*o*NBA (250 kDa)/10% fGel were cast into PDMS rings (6 mm internal diameter, 1.5 mm height, 40 μL per sample). Samples (n = 3) were irradiated for 5 min (365 nm, 20 mW cm^{-2}), removed from the PDMS molds, and weighted (m_0). Crosslinked hydrogels were left to swell in PBS (6 mL per gel) in 6-well plates under gentle shaking. After 24 h, the samples were weighted (m_s, swollen state) and finally freeze-dried to obtain the dry-mass (m_d). Their swelling and swelling % were calculated by:

$$\text{Swelling} = \frac{m_s}{m_d}$$

$$\text{Swelling}\,\%(\text{solvent uptake}) = \frac{m_s - m_0}{m_0} \times 100$$

Adhesion tests

Lap-shear and tensile tests were performed on a Discovery HR 20 (TA instruments) equipped with tensile grip geometries. For lap-shear tests, the porcine skin (Stellen Medical LLC, Fisher Scientific) was cut in 3 × 1 cm^2 slices and 40 μL of fibrin sealant (Tisseel, Baxter) or 2.5% HA-*o*NBA/10% fGel or 2.5% HA*o*NBA/10% fGel-SH were pipetted on a 1 × 1 cm surface (dermis side). A second slice (facing dermis side) was gently pressed on top of the first one and adhered using either a fibrin sealant or UV cured using an Omnicure Series2000 lamp (Lumen Dynamics) at 365 nm for 5 min at 20 mW cm^{-2}. Tensile test samples were prepared similarly using 1 cm circular porcine skin cuts previously attached to metal substrates using cyanoacrylate superglue. Samples were then fixed on the tensile grips and then pulled away at 20 μm s^{-1} speed. The maximum pulling force recorded was divided over the contact area (1 cm^2 for lap-shear, 0.785 cm^2 for tensile) and plotted as adhesive strength.

Reactive oxygen species (ROS) assays

Photoresins (Fig. 3B and 4B) were prepared as described above. In addition, a 0.75% alginate solution was prepared as radical-free, ionic crosslinking-based negative control. Foreskin human fibroblasts were cultured in FBS-free DMEM media for 24 h prior to the experiment. The photoresins were mixed with fibroblasts (passage 7–9) to a final concentration of 2.5 million cells mL^{-1}. The bioresins were then casted in a 96-well plate (80 μL per well) and crosslinked with a 5-minute light irradiation (365 nm, 20 mW cm^{-2}). The alginate formulation was crosslinked by addition of 25 mM calcium chloride ($CaCl_2$) solution. Samples were then incubated in serum-free DMEM with or without (background fluorescence) ROS assay fluorogenic component (abcam186028, abcam) at 20 mM. After 4 h, the fluorescence intensity was detected with 530 nm excitation and 590 nm emission using a BioTek Synergy HT plate reader set at 37 °C. Intracellular relative fluorescence was quantified by comparing the fold increase of the samples with ROS fluorogenic component to the samples without it. Samples were also imaged on a confocal microscope (Imager Z2, Zeiss) equipped with a water-immersion objective (10×/0.3). For the photoresins of Fig. 4B, deep-red ROS assay fluorogenic test (abcam186029, abcam) was instead used (620 nm excitation, 680 nm emission) to avoid overlap absorption with the Ru/SPS (Advanced Biomatrix) initiating system.

Live/dead assays

HA-SH (DS: 10%, 250 kDa) and HA-MA (DS: 10%, 250 kDa) were dissolved at 2% in PBS. PEG4*o*NBA (20 kDa) was dissolved at 20% in DMSO, PEG4SH (20 kDa) and PEG4MA (20 kDa) at 20% in PBS, and LAP at 2% PBS. The polymer solutions were then mixed to obtain the formulations presented in Fig. 4B. These photoresins were then filter sterilized (0.2 μm filter) and mixed with foreskin human fibroblasts (passage 7–9) to a final concentration of 2.5 million cells mL^{-1}. The bioresins were casted in PDMS rings (4 mm diameter, 1 mm height, 15 μL per sample) previously sterilized *via* 70% ethanol and UV treatment and positioned in 48-well plates. The samples were irradiated for 5 min (365 nm, 20 mW cm^{-2}) and then cultured in DMEM with 10% v/v FBS and antibiotic-antimycotic (100 units per mL penicillin, 100 μg mL^{-1} streptomycin, and 0.25 μg mL^{-1} Gibco Amphotericin B) with media change every other day. Cells-embedded hydrogels (n = 3) were taken at day 0 (4 h after crosslinking), day 2, and day 7 and incubated in phenol red-free DMEM supplemented with 1 : 2000 calceinAM and 1 : 500 ethidium homodimer-1 for 45 min. Imaging (200 μm, 10 μm steps) was performed on a confocal microscope (Imager Z2, Zeiss) equipped with a water-immersion objective (10×/0.3). Cell viability was quantified by counting viable (calcein) and dead (ethidium homodimer-1) cells with the ImageJ Analyze particle function. The same procedure was followed for the 2.5% HA-*o*NBA/10% fGel formulation.

Vascular organoids

Early-stage vascular organoids were generated from BJFF hiPSCs[35] following a reported protocol.[36] Briefly, single-cell hiPSCs suspensions were aggregated overnight into embryoid bodies (EBs) roughly 100–150 μm in diameter. These EBs were differentiated in N2B27 medium to produce early-stage vascular organoids.[36] The media was supplemented with 12 μM CHIR 99021 (#2520691, BioGems) and 25 ng mL^{-1} BMP4 (3130-111-165, Miltenyi Biotech) for 3 days, followed by 2 days of supplementation with 100 ng mL^{-1} VEGF (hVEGF-A 165, #100-20, ThermoFisher) and 2 μM Forskolin (#F3917, Sigma). After sedimentation the organoids in a conical tube and removing the excess media, the vascular organoids were gently mixed with the 1.3% PEG4*o*NBA/1% HA-SH photoresin using 1 mL wide-bore opening tips (Axygen). Single drops of these bioresins were crosslinked in a 48-well plate and cultured in EGM-2 complete media (Lonza Biosciences) for 3 days. For hydrogel dissolution, media was supplemented with 1 M cysteine. Images were taken on a Leica DM IL LED microscope.

3D printing

The photo-ink 1.3% PEG4*o*NBA/1% HA-SH (250 kDa, DS: 10%) was prepared as previously described and photocrosslinked at

365 nm and 20 mW cm^{-2} for 5 min. The hydrogel was then loaded into a 3-cc UV/light block amber cartridge (Nordson EFD). The cartridge was centrifuged at 3000 rpm for 10 min to compact the dynamic polymer network and eliminate air bubbles. H-shaped structures were 3D printed using a pneumatic-driven extrusion on a 3-axis motion-controlled stage (Aerotech). An ink reservoir is mounted on the printer using a custom-machined syringe holder. The ink is extruded through a plastic tapered nozzle (Nordson EFD; 410 μm diameter) with pneumatic pressure of 2 psi (~14 kPa) using digital pressure controllers (PCD-100PSIG-D, Alicat Scientific) and translated at a speed of 2.5 mm s^{-1}. The G-code for the printed structure was generated using a custom Python code.

Projection-based photocrosslinking

The photoresin composed of 2.5% HA-*o*NBA (250 kDa)/10% fGel was prepared as previously described and pipetted on a glass slide. Photo-masks were printed *via* digital-light processing (DLP, Elegoo Mars 2P) and positioned between the light source (Omnicure Series2000 lamp, Lumen Dynamic) featuring a 365 nm bandpass filter and the sample. Samples were irradiated for 60 s and then washed with PBS to remove any uncured resin. Upon removal of PBS, optical images of the printed hydrogels were taken.

Materials

All chemicals were purchased from Merck, and cell culture reagents from ThermoFisher Scientific unless otherwise specified. Thiol, amine and methacrylate terminated PEGs were purchased from Creative PEGworks.

Statistical analysis

Data are reported as mean values ± SDs (n = 3). Statistical analysis is performed using GraphPad Prism 9 and statistical significance is determined using one-way Anova with multiple comparisons or unpaired Welch's t-test.

Results and discussion

Amide *o*NBA-based chemistry

We first synthesized a monofunctional linear molecule (m-*o*NBA) featuring a reactive end and a short ethoxy chain (Fig. 1B, ESI Fig. S3 and 4†). A solution of 10 mM m-*o*NBA in water was exposed to UV light (365 nm, 20 mW cm^{-2}), and the decay of its concentration upon photolysis was monitored over time by LC-MS (Fig. 1B-I). Upon photoexcitation, *o*NBA undergoes photolysis to an *o*-nitrosobenzaldehyde (activated *o*NBA) with reactive nitroso and aldehyde groups (Fig. 1A-I). The consumption of m-*o*NBA is roughly 40%, 65% and 90% after 60 s, 120 s, and 300 s of light exposure, respectively. The reactivity of photoactivated *o*NBA with thiols and amines is measured by HPLC using solutions containing m-*o*NBA with either *O*-(2-mercaptoethyl)-*O*′-methyl-hexa(ethylene glycol) as monofunctional thiol (m-SH) or 2-(2-(2-ethoxyethoxy)ethoxy)ethanamine as monofunctional amine (m-NH_2) (Fig. 1B-II and ESI Fig. S15–19†). In both cases, the m-*o*NBA peak reduces dramatically over 300 s of light exposure due to either the formation of a *N*-semimercaptal adduct *via* the reaction between m-*o*NBA and m-SH or an indazolone adduct *via* the reaction between m-*o*NBA and m-NH_2.

Absorption spectra of the amide m-*o*NBA and its photolysis products reveal a significant difference in their molar extinction coefficient (Fig. 1B-III). In particular, m-*o*NBA displayed an absorbance at 365 nm (41.5 M^{-1} cm^{-1}) that is significantly lower than that of lithium phenyl-2,4,6-trimethylbenzoylphosphinate (LAP), the current gold-standard for bioprinting.[3] We note that the absorbance is comparable to that of LAP at 405 nm (47 M^{-1} cm^{-1}). Upon photolysis, the absorption of these reaction mixtures increases significantly, reaching values between 200 and 400 M^{-1} cm^{-1}. Hence, the competitive absorption of the *o*NBA photoproducts acts as an internal filter reducing photolysis efficiency, especially for highly concentrated photoresins. Interestingly, we also observe a significant difference between the absorption profiles of *N*-semimercaptal and indazolone adducts, particularly at λ < 350 nm and λ > 400 nm. This observation is consistent with their structural differences, which impact the electronic environment of the adjacent aromatic core.

Thiolated and amine-based synthetic hydrogels

To produce synthetic hydrogels, we created a four-arm polyethylene glycol crosslinker terminated with amide *o*NBA (PEG4*o*NBA) (ESI Fig. S5†). The photopolymerization of PEG4*o*NBA in the presence of thiolated (PEG4SH) or amine-terminated (PEG4NH_2) four-arm PEGs is assessed by oscillatory photorheology (365 nm, 20 mW cm^{-2}) (Fig. 1C). As controls, we also generated synthetic hydrogels using a methacrylated four-arm PEG (PEG4MA) (chain-growth mechanism) as well as norbornene and alkyne terminated four-arm PEGs (PEG4NB, PEG4yne) (step-growth mechanism). For these control photoresins, LAP is used as a photoinitiator (0.05% w/v). As expected, the highly efficient thiol–norbornene photoclick chemistry exhibits both fast crosslinking kinetics and improved mechanical properties. *S*-Nitrosylation (thiol-*o*NBA), akin to recent observations by Zhou *et al.*,[37] showed surprisingly fast kinetics that are comparable to photoinitiator-based methacrylate and thiol–yne chemistries (Fig. 1C). Thiol-*o*NBA hydrogels also resulted in higher storage modulus, G' = 2855 ± 392 Pa *vs.* G' = 2048 ± 127 Pa for thiol–yne, and G' = 1251 ± 144 Pa for methacrylate, suggesting a higher crosslinking density and, hence, better reaction yield. By contrast, the less efficient indazolone-based photoresin (amine-*o*NBA) exhibited a significantly delayed gelation onset and lower G' = 533 ± 121 Pa.

The rapid nucleophilic addition reaction between a primary thiol and the aryl nitroso group (*S*-nitrosylation) of activated *o*NBA is responsible for the formation of *N*-semimercaptal crosslinking sites (Fig. 2A).[37–39] *S*-Nitrosylation is a common reaction that occurs in human cells for reversible cell signaling, with nitric oxide (NO) reacting with the thiol group of cysteine side chains in proteins.[40,41] On the other hand, the presence of an electron-withdrawing amide group has been

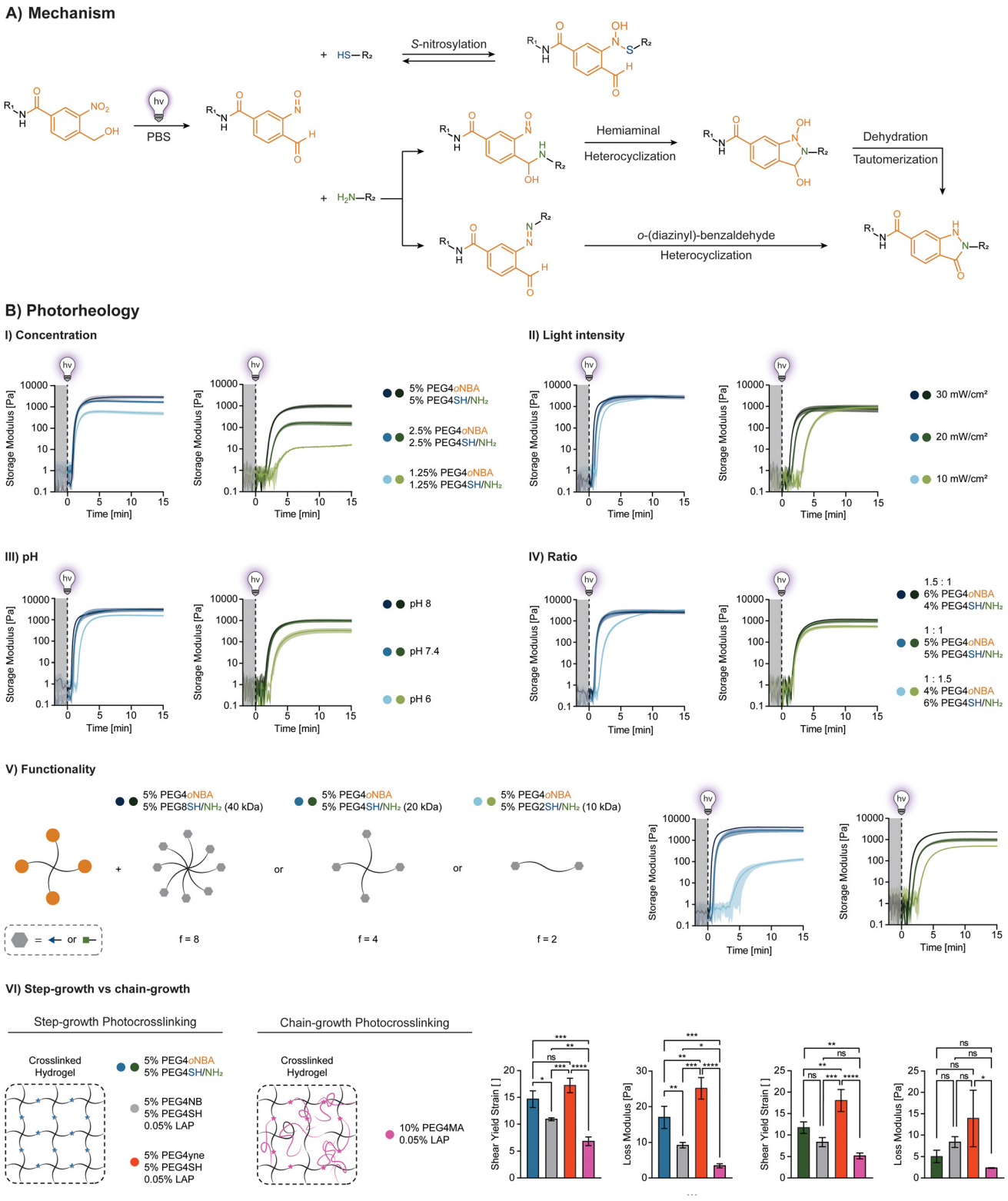

Fig. 2 (A) Schematics of thiol-*o*NBA (top) and amine-*o*NBA (bottom) reaction mechanisms. Upon *o*NBA photolysis, thiol addition to the nitroso group (*S*-nitrosylation) leads to the formation of a dynamic *N*-semimercaptal bond, while an amine addition to the benzaldehyde or nitroso group results in hemiaminal or *o*-(diazinyl)-benzaldehyde, respectively. The more stable indazolone bond forms upon the additional steps of dehydration, tautomerization, and heterocyclization. (B) Photorheology data (semilog plots of *G*′ *vs.* time) highlight the influence of polymer concentration (I), light intensity (II), pH (III), ratio (IV), and polymer functionality (V) on thiol-*o*NBA and amine-*o*NBA photocrosslinking. Synthetic hydrogels formed by step-growth (thiol–norbornene, thiol–yne, thiol-*o*NBA and amine-*o*NBA) exhibit higher loss moduli, *G*″ and higher yield shear stress compared to those generated by chain-growth (methacrylate) photocrosslinking (VI).

shown to confer *o*NBA excellent reactivity towards primary amines *via* the formation of an indazolone bond.[33] As highlighted by Zhu *et al.*,[42] indazolone formation can proceed *via* condensation at the nitroso group to form a diazine intermediate or, although not thermodynamically favored, at the benzaldehyde to form a hemiaminal intermediate (Fig. 2A). Both intermediates then undergo heterocyclization (and dehydration and tautomerization in the case of hemiaminal) to form the more stable indazolone.

Next, we investigated the influence of different parameters on the performance of *S*-nitrosylation and indazolone photocrosslinking (Fig. 2B). As expected, hydrogel stiffness increases with polymer concentrations (Fig. 2B-I, ESI Fig. S20 and 21†). Increasing the irradiation light intensity from 10 to 30 mW cm^{-2} significantly accelerated the photoresin gelation (from ~180 s to 60 s for thiol-*o*NBA, and from ~330 s to 120 s for amine-*o*NBA), while leading to similar mechanics (Fig. 2B-II, ESI Fig. S20 and 21†).

The pH of the reaction mixture also influences photocrosslinking (Fig. 2B-III, ESI Fig. S20 and 21†). In particular, the reaction proceeds significantly faster in an alkaline environment (pH 8), in good agreement with the proposed reaction mechanisms. For thiol-*o*NBA, as with thiol-Michael addition, increasing the pH results in the presence of a higher ratio of reactive, deprotonated thiols (thiolate anions). Conversely, in an acidic environment (pH 6), the lower thiolate ratio limits the crosslinking rate resulting in a significantly lower hydrogel stiffness. A decrease in crosslinking efficiency in acidic environment (pH 6) is also observed for amine-*o*NBA, in agreement with the nucleophilic addition first step, and in contrast to the possible formation of an unstable imine (favored at pH 5–6). Importantly, physiological pH 7.4 results G' values comparable to those observed under alkaline conditions. Finally, the molar ratio of *o*NBA : SH/NH_2 plays a key role, with 1 : 1 and 1.5 : 1 ratios resulting in faster gelation relative to hydrogels with excess thiols or amines (1 : 1.5) (Fig. 2B-IV, ESI Fig. S20 and 21†).

It is well known that increasing polymer functionality (reactive groups per polymer chain) is an effective way to accelerate the onset of gelation.[43,44] When using thiolated PEGs with the same distance between two functional groups (10 kDa) and concentration, the thiol/amine-*o*NBA crosslinking kinetics improve with increasing thiol/amine functionality (2, 4, and 8) (Fig. 2B-V, ESI Fig. S20 and 21†). To gain further insight, we compared their behavior to hydrogels obtained *via* step-growth (thiol–norbornene, thiol–yne) and chain-growth (methacrylate) chemistries (Fig. 2B-VI). Each photoresin contains the same molecular weight, concentration, and functionality, resulting in the same G' values. The thiol-*o*NBA network exhibits a loss modulus G'' of 16.97 ± 2.54 Pa which lies between that observed for thiol–norbornene, G'' = 9.24 ± 0.63, and thiol–yne, G'' = 25.15 ± 2.48, and it is roughly 5-fold higher than the heterogeneous chain-growth methacrylate network, G'' = 3.42 ± 0.47, suggesting a step-growth mechanism. Moreover, the thiol-*o*NBA network exhibited a 2-fold higher yield shear strain compared to the more brittle chain-growth system. Together, these observations support our hypothesis that *S*-nitrosylation leads to homogeneous (step-growth) synthetic hydrogels with improved mechanical properties compared to the established methacrylic systems. The amine-*o*NBA gelation also proceeds *via* a step-growth process, in which a significantly higher (2-fold) yield strain is observed for these hydrogels compared to chain-growth methacrylic hydrogels (Fig. 2B-VI).

Overall, we observed similar trends between the two chemistries (thiol-*o*NBA and amine-*o*NBA), consistent with their similar nucleophilic addition process and step-growth network formation. However, due to the intrinsically less efficient amine-*o*NBA reaction, the crosslinking kinetics are significantly slower (~1.5–2×) than thiol-*o*NBA for the conditions tested. In particular, the decrease in polymer concentration and functionality had a more drastic effect on their storage modulus compared to those based on thiol-*o*NBA chemistry, suggesting that proximity of functional groups plays an important role in ensuring the desirable performance of amine-*o*NBA photoresins.

Dynamic hydrogel networks

To create biocompatible hydrogels, thiolated hyaluronic acids (HA-SH) with the same degree of substitution (DS ~ 10%) and varying molecular weight (100 kDa, 250 kDa, 2 MDa) are synthesized, resulting in functionalities ranging from ~25 to ~500. As expected, increasing thiol functionality dramatically increases gelation kinetics (Fig. 3A), enabling gelation at low polymer content (1% HA-SH). Interestingly, no improvement is observed using 2 MDa HA-SH. We hypothesize that this arises due to the rapid formation of intramolecular disulfide bonds (not involved in *S*-nitrosylation), as supported by their gelation in air (spontaneous oxidation of thiols). The swelling behavior of soft thiol-*o*NBA hydrogels with optimized photoresin (1.3% PEG4*o*NBA/1% HA-SH 250 kDa) was also characterized (ESI, Fig. S22†).

For applications of interest, thiol-*o*NBA must be biocompatible. To first confirm that the thiol-*o*NBA reaction proceeds *via* a radical-free process, the optimized photoresin composed of 1.3% PEG4*o*NBA/1% HA-SH (250 kDa) is used to perform a ROS assay in the presence of human dermal fibroblasts (Fig. 3B-I). Photoresins composed of 1.3% PEG4NB/1% HA-SH, 1.3% PEG4yne/1% HA-SH, and 1.3% PEG4MA/1% HA-MA are used as radical-mediated controls in the presence of 0.035% LAP. Alginate is used as a radical-free control (ionic crosslinking mechanism). After exposure to 365 nm light (20 mW cm^{-2}) for 5 min, the formation of ROS in the photoinitiator-based system resulted in a significant increase in intracellular fluorescence. Likely due to chain propagation during the chain-growth process, the methacrylate resin exhibited ROS levels 2× and 10× higher than the more efficient step-growth thiol–yne and thiol–norbornene chemistries, respectively. By contrast, the thiol-*o*NBA system exhibits a fluorescence level comparable to that of alginate, indicative of a radical-free process. Confocal imaging further highlights the presence or absence of ROS-positive (fluorescent) cells in these samples. The accumulation of intracellular ROS is known to harm cells, altering their redox state and proliferative capacity, and poten-

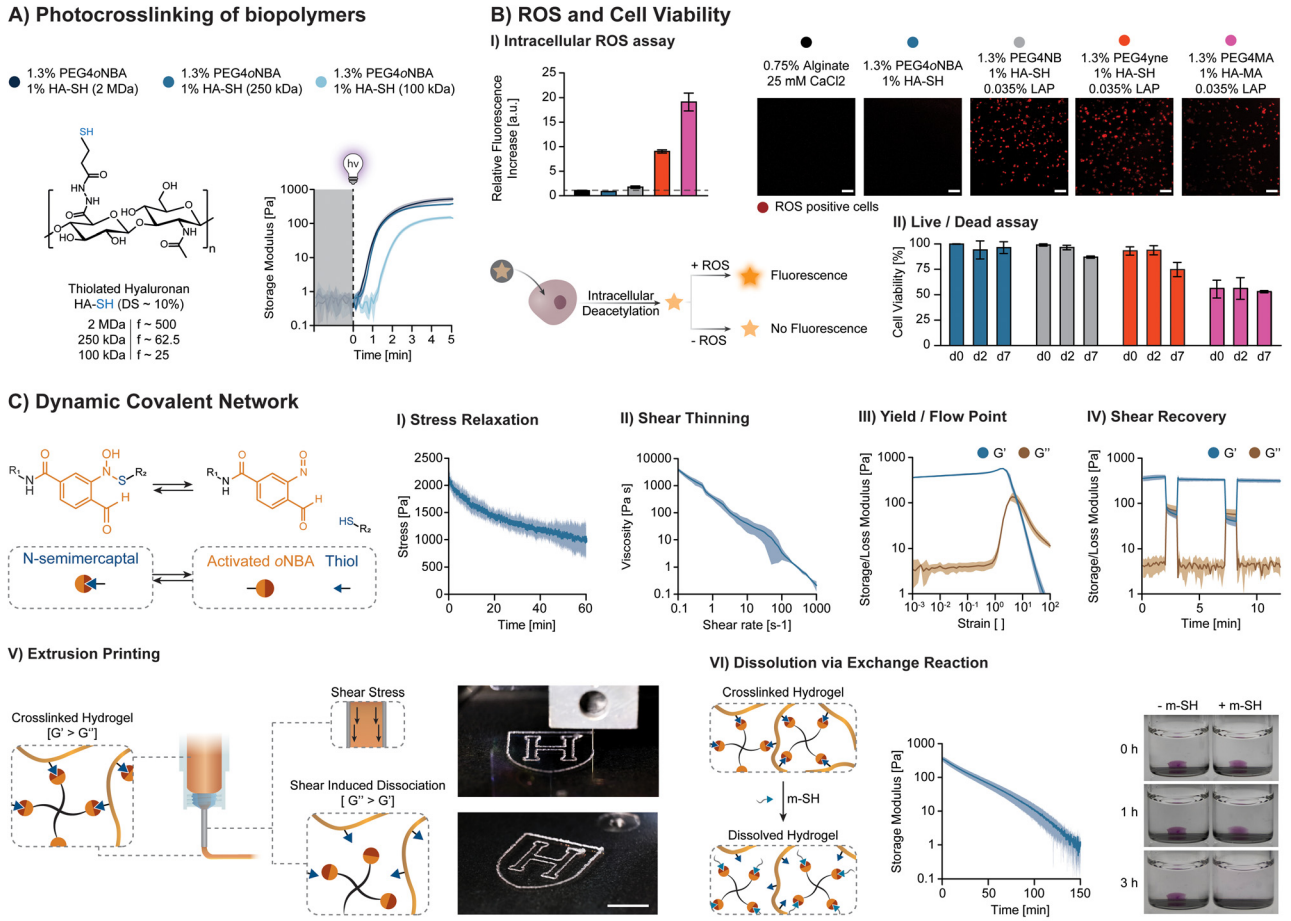

Fig. 3 (A) Photocrosslinking and photorheology of thiolated hyaluronic acid (HA-SH) *via* thiol-*o*NBA, in which crosslink kinetics increase with increasing functionality. [Note: the use of 2 MDa HA-SH did not lead to significant improvement compared to 250 kDa HA-SH, possibly due to the formation of disulfide bonds that are inactive towards *S*-nitrosylation.] (B) Fluorescent reactive oxygen species (ROS) assay confirms the radical-free nature of the thiol-*o*NBA crosslinking compared to free-radical chemistries, *i.e.*, thiol–norbornene, thiol–yne, and methacrylate. The methacrylate resin showed significantly higher ROS-derived fluorescence, possibly due to the intrinsic nature of the chain-growth mechanism (kinetic chain propagation). Alginate is used as a negative control (radical-free, ionic crosslinking process) (I). Live/dead assay reveals good biocompatibility of the thiol-*o*NBA resin upon printing (day 0) and improved cell viability over a 2- and 7-day culture period compared to other photochemistries (II). (C) *N*-semimercapal hydrogel (1.3% PEG4oNBA/1% HA-SH 250 kDa) exhibits characteristic mechanical properties of a dynamic hydrogel network, including stress relaxation (I), shear thinning (II), flow point (III), and shear recovery (IV). This shear-induced bond dissociation enables extrusion-based printing of thiol-*o*NBA photo-ink. Scale bar: 1.5 cm (V). Hydrogels with dynamic bonds exhibit on-demand dissolution in the presence of excess monofunctional thiol (m-SH), as reflected by the decrease in *G'* as a function of time (or visually with rhodamine-grafted hydrogels).

tially inducing differentiation.[11,45] Importantly, these results are in agreement with recent studies that indicate low intensity (≤50 mW cm^{-2}), near-UV (≥365 nm) irradiation is safe for cells, and oxidative damage arises from radical initiating species.[11,45] Hence, the radical-free nature of the *S*-nitrosylation reaction represents a distinct performance advantage over existing alternatives. Moreover, in agreement with the ROS assay results, excellent cell viability (>95%) is achieved for the radical-free thiol-*o*NBA hydrogel, while among the free-radical photoinitiator-based systems, the methacrylate resin showed the lowest viability over one week of culture (~50%), followed by thiol–yne (~75%) and thiol–norbornene (~87%) (Fig. 3B-II and ESI, Fig. S23†).

The dynamic nature of the *N*-semimercaptal covalent bond confers additional performance advantages (Fig. 3C). Unlike covalent gels, their dynamic bonding can facilitate cell migration, spreading and tissue development.[22,24,46–48] The stress-relaxation behavior of *N*-semimercaptal hydrogels is of interest for biomimetic dynamic hydrogel matrices (Fig. 3C-I). These hydrogels also exhibit shear thinning (Fig. 3C-II), shear recovery (Fig. 3C-IV), and the presence of a shear-induced flow point (Fig. 3C-III) and can be therefore exploited as photosensitive inks (photo-inks) for extrusion printing. When the thiol-*o*NBA hydrogel is extrusion-based printed through a fine nozzle, the induced shear stress disrupts the *N*-semimercaptal bonds facilitating the photo-ink flow. Upon deposition, the photo-ink returns to a quiescent (shear-free) state and these bonds rapidly reform within the *N*-semimercaptal hydrogel (Fig. 3C-V). These dynamic bonds can also be exploited to induce a gel-to-fluid transition in the presence of monofunc-

tional thiols (m-SH). m-SH can compete with the thiolated polymer for the addition to the nitroso group of the activated *o*NBA without contributing to network formation, promoting hydrogel dissolution over time (Fig. 3C-VI). One potential application that we envision for these biocompatible, viscoelastic hydrogels is the encapsulation of human cells, spheroids, and organoids and their subsequent release *via* on-demand dissolution (ESI, Fig. S24†).

Pristine protein networks

A major advantage of amide *o*NBA resides in its reactivity towards primary amines, which are abundant in native extracellular matrices. We investigated whether *o*NBA-based crosslinkers can be used to form hydrogels from pristine proteins containing lysine residues (Fig. 4A). As an example, unmodified fish gelatin (fGel) is used to form hydrogels in the presence of PEG4*o*NBA and light exposure. Despite the relatively high polymer concentration (5% fGel + 5% PEG4*o*NBA), photocrosslinking results in soft hydrogels (G' = 378 ± 19 Pa) due to the low efficiency of amine-*o*NBA reaction combined with low lysine content and accessibility in fGel. To improve their performance, we synthesized *o*NBA-modified HA (HA*o*NBA) and increased the functionality of the *o*NBA crosslinker from 4 (PEG4*o*NBA) to 25 (HA*o*NBA 100 kDa) and 62.5 (HA*o*NBA 250 kDa), which dramatically improved both gelation kinetics and mechanical properties (Fig. 4A-II). The swelling behavior of amine-*o*NBA hydrogels with optimized photoresin (2.5% HA*o*NBA 250 kDa, 10% fGel) was also characterized (ESI, Fig. S25†)

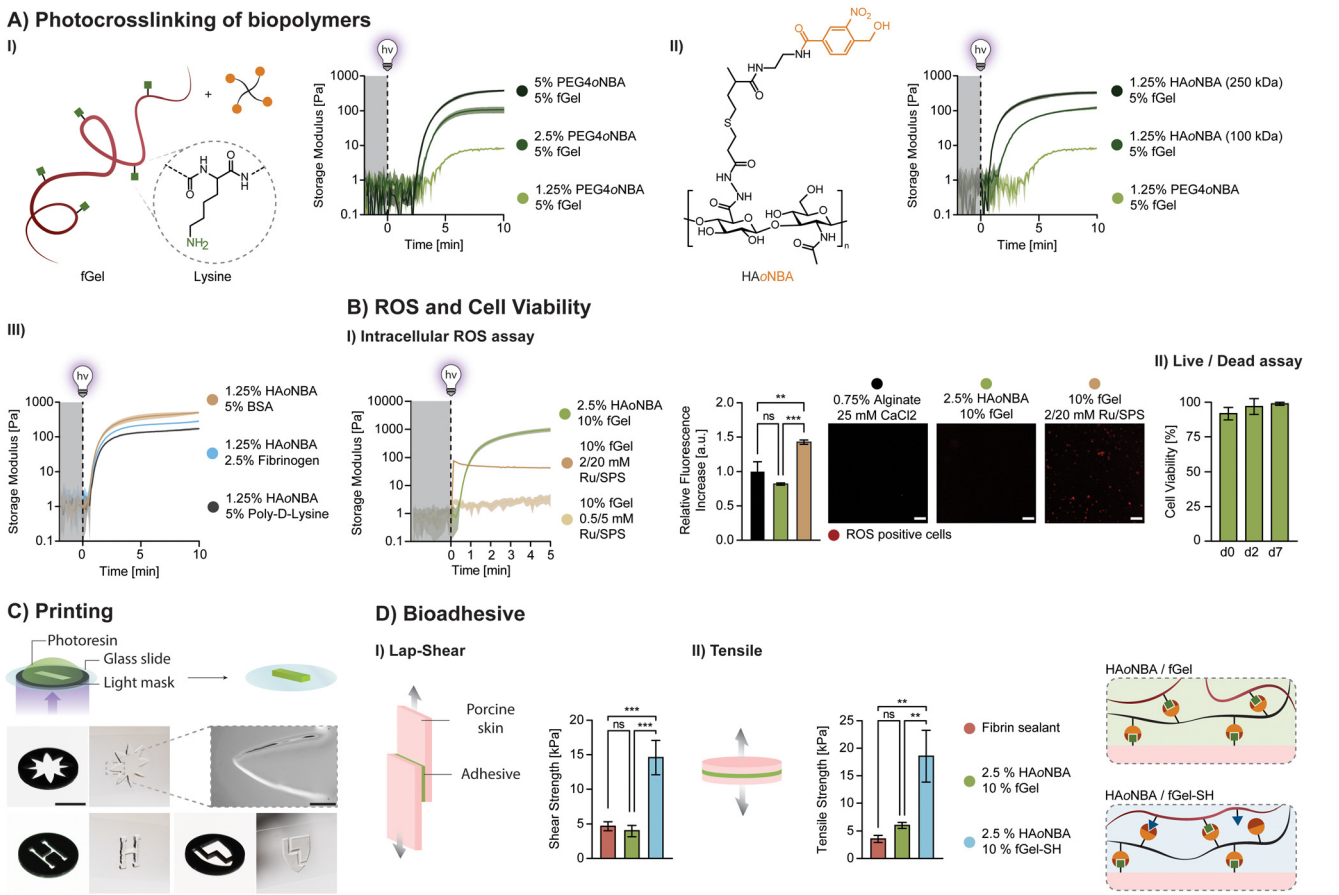

Fig. 4 (A) Photocrosslinking and photorheology of fish gelatin (fGel) *via* amine-*o*NBA, in which increasing PEG4*o*NBA crosslinker concentration improves gelation kinetics and hydrogel stiffness (I). Enhanced crosslinking kinetics and stiffness is observed when using *o*NBA-modified HA (HA*o*NBA) as high-functionality crosslinker even at a low concentration (1.25%) (II). Photorheology of hydrogel networks composed of amine-bearing proteins, including unmodified bovine serum albumin (BSA) and fibrinogen (III). (B) Fluorescent reactive oxygen species (ROS) assay confirming the radical-free nature of the amine-*o*NBA crosslinking compared to tyrosine oxidation chemistry based on the use of the bimolecular photoinitiator systems Ru/SPS. Alginate is used as a negative control (radical-free, ionic crosslinking process). Possibly due to the low abundancy of tyrosine residues, Ru/SPS-based crosslinking was shown to be much less efficient than amine-*o*NBA yielding ultra soft hydrogels (G' < 100 Pa) (I). Live/dead assay showing excellent biocompatibility of the amine-*o*NBA resin at day 0 (>90%), day 2 and day 7 (>95%) (II). (C) Projection-based printing *via* photo-masks (flower, H, and logo) showing spatio-temporal control over photocrosslinking of amine-*o*NBA photoresin (2.5% HA*o*NBA/10% fGel). Close up of flower petal reveals a resolution ~250 μm at its tip. Scale bars: 10 mm, close up 1 mm. (D) Bioadhesive *o*NBA photoresins exploit reactivity with amine-rich porcine skin tissue. Photoresin composed of 2.5% HA*o*NBA/10% fGel exhibits shear (I) and tensile (II) adhesive strengths on porcine skin (dermis) comparable to a clinically used commercial fibrin sealant. The use of thiolated fGel (fGel-SH) gives rise to a 3- to 4-fold increase in adhesive strength, outperforming a commercial fibrin sealant.

Exploiting the high reactivity of HA*o*NBA (250 kDa), we explored crosslinking of other amine-rich polymers (Fig. 4A-III), demonstrating unprecedented ease and versatility in photocrosslinking unmodified proteins for potential biological applications. Importantly, nitrobenzyl-based crosslinkers are used to generate hydrogels in the presence of amine-containing polymers *via* imine formation. However, since imine crosslinking is generally slow and results in soft, unstable gels, it has often been coupled with a more robust crosslinking strategy (*i.e.*, methacrylate).[30,31] We showed that due to the amide-grafted *o*NBA residue, the favored indazolone linkage ensures hydrogel stability over time. Photocrosslinked hydrogels (2.5% HA*o*NBA, 10% fGel) maintain a stable storage modulus over time in the presence of excess monofunctional amine (1 M Glycine, m-NH_2), comparable to control hydrogels left in PBS (ESI, Fig. S26†).

An alternate photocrosslinking strategy for unmodified proteins is based on photooxidation with a ruthenium type II bimolecular photoinitiator composed of tris(2,2′-bipyridine) ruthenium(II) and co-initiator sodium persulfate (Ru/SPS).[49–51] Since the photooxidation of the Ru/SPS system drives the dimerization of tyrosine residues, it works with tyrosine-rich polymers, including both silk sericin/fibroin[49] and other extracellular matrices.[50] However, when used to crosslink 10% fGel, Ru/SPS yields ultrasoft gels (G' < 100 Pa) at high concentration (2 mM Ru, 20 mM SPS) and lightly crosslinked networks (G' < 10 Pa) at low concentration (0.5 mM, 5 mM SPS) (Fig. 4B-I). Unlike the radical-free amine-*o*NBA mechanism, the Ru/SPS system generates initiating radical species upon light excitation, as confirmed by the ROS assay (Fig. 4B-I).

Importantly, the optimized amine-*o*NBA photoresin (2.5% HA*o*NBA/10% fGel) is biocompatible. For example, human neonatal dermal fibroblasts (HNDFs) encapsulated within this hydrogel exhibited excellent cell viability (>95%) during a 7-day culture period (Fig. 4B-II and ESI Fig. S27†).

To demonstrate spatio-temporal control over the photocrosslinking process, we designed photo-masks for projection-based printing of three motifs. Higher magnification imaging of the flower tip reveals a minimum resolution of ~250 μm (Fig. 4C). These initial findings demonstrate the feasibility of using amine-*o*NBA chemistry for photolithographic-based methods, such as digital light processing (DLP). Finally, to assess bioadhesion, we carried out lap-shear and tensile tests on porcine skin (dermis) for the 2.5% HA*o*NBA/10% fGel formulations. These matrices exhibit an adhesive strength comparable to a commercially available fibrin sealant, which is widely used in sutureless surgical procedures (Fig. 4CI-II). Remarkably, the bioadhesive properties of thiolated fGel (fGel-SH) are 3–4 fold higher than this fibrin sealant.

Conclusions

In summary, we have demonstrated that amide *o*NBA can be used as a photoinitiator- and radical-free moiety for creating synthetic and biological hydrogels *via* light-mediated crosslinking. Our approach enables an unprecedented combination of performance advantages over traditional photochemistries, including synthetic hydrogels with dynamic bonds (thiol-*o*NBA) and those composed of pristine proteins (amine-*o*NBA) with high cell viability and bioadhesion. This radical-free chemistry reveals that radical species leading to cellular oxidative stress are primarily responsible for cell death, not low dose, near-UV light. Our work paves the way for myriad applications ranging from cell/organoid encapsulation to bioprinted human tissues.

Author contributions

R. R. and J. A. L. designed research; R. R., J. K. W. and A. J. A. performed research; R. R., and D. M. B. analyzed data; R. R. and J. A. L. wrote the paper.

Data availability

Data for this article are available at Harvard Dataverse at **https://doi.org/10.7910/DVN/T4EYXJ**.

Conflicts of interest

J. A. L. serves on the Scientific Advisory Boards of Azul 3D and Trestle Biotherapeutics.

Acknowledgements

This work was supported by the Vannevar Bush Faculty Fellowship Program sponsored by the Department of the Navy, Office of Naval Research (N00014-21-1-2958). R. R. acknowledges Swiss National Science Foundation Postdoc.Mobility fellowship (P500PM_214191). The use of the BJFF-hiPSC line is made possible by the Kidney Translational Research Center (KTRC) and the ATLAS D2K (U24DK135157) and WU-PCEN (P50DK133943) grants.

References

1 T. E. Brown and K. S. Anseth, Spatiotemporal hydrogel biomaterials for regenerative medicine, *Chem. Soc. Rev.*, 2017, **46**(21), 6532–6552, DOI: **10.1039/C7CS00445A**.
2 L. Li, J. M. Scheiger and P. A. Levkin, Design and Applications of Photoresponsive Hydrogels, *Adv. Mater.*, 2019, **31**(26), 1807333, DOI: **10.1002/adma.201807333**, (acccessed 2024/03/21).
3 M. Lee, R. Rizzo, F. Surman and M. Zenobi-Wong, Guiding Lights: Tissue Bioprinting Using Photoactivated Materials, *Chem. Rev.*, 2020, **120**(19), 10950–11027, DOI: **10.1021/acs.chemrev.0c00077**.

4 C. Yu, J. Schimelman, P. Wang, K. L. Miller, X. Ma, S. You, J. Guan, B. Sun, W. Zhu and S. Chen, Photopolymerizable Biomaterials and Light-Based 3D Printing Strategies for Biomedical Applications, *Chem. Rev.*, 2020, **120**(19), 10695–10743, DOI: 10.1021/acs.chemrev.9b00810.

5 R. Levato, O. Dudaryeva, C. E. Garciamendez-Mijares, B. E. Kirkpatrick, R. Rizzo, J. Schimelman, K. S. Anseth, S. Chen, M. Zenobi-Wong and Y. S. Zhang, Light-based vat-polymerization bioprinting, *Nat. Rev. Methods Primers*, 2023, **3**(1), 47, DOI: 10.1038/s43586-023-00231-0.

6 H. Liu, P. Chansoria, P. Delrot, E. Angelidakis, R. Rizzo, D. Rütsche, L. A. Applegate, D. Loterie and M. Zenobi-Wong, Filamented Light (FLight) Biofabrication of Highly Aligned Tissue-Engineered Constructs, *Adv. Mater.*, 2022, **34**(45), 2204301, DOI: 10.1002/adma.202204301, (acccessed 2023/02/16).

7 M. Regehly, Y. Garmshausen, M. Reuter, N. F. König, E. Israel, D. P. Kelly, C.-Y. Chou, K. Koch, B. Asfari and S. Hecht, Xolography for linear volumetric 3D printing, *Nature*, 2020, **588**(7839), 620–624, DOI: 10.1038/s41586-020-3029-7.

8 B. E. Kelly, I. Bhattacharya, H. Heidari, M. Shusteff, C. M. Spadaccini and H. K. Taylor, Volumetric additive manufacturing via tomographic reconstruction, *Science*, 2019, **363**(6431), 1075–1079, DOI: 10.1126/science.aau7114, (acccessed 2023/02/20).

9 D. Loterie, P. Delrot and C. Moser, High-resolution tomographic volumetric additive manufacturing, *Nat. Commun.*, 2020, **11**(1), 852, DOI: 10.1038/s41467-020-14630-4.

10 J. M. Kronenfeld, L. Rother, M. A. Saccone, M. T. Dulay and J. M. DeSimone, Roll-to-roll, high-resolution 3D printing of shape-specific particles, *Nature*, 2024, **627**(8003), 306–312, DOI: 10.1038/s41586-024-07061-4.

11 R. Rizzo, N. Petelinšek, A. Bonato and M. Zenobi-Wong, From Free-Radical to Radical-Free: A Paradigm Shift in Light-Mediated Biofabrication, *Adv. Sci.*, 2023, **10**(8), 2205302, DOI: 10.1002/advs.202205302, (acccessed 2024/01/18).

12 E. R. Ruskowitz and C. A. DeForest, Proteome-wide Analysis of Cellular Response to Ultraviolet Light for Biomaterial Synthesis and Modification, *ACS Biomater. Sci. Eng.*, 2019, **5**(5), 2111–2116, DOI: 10.1021/acsbiomaterials.9b00177.

13 N. E. Fedorovich, M. H. Oudshoorn, D. van Geemen, W. E. Hennink, J. Alblas and W. J. A. Dhert, The effect of photopolymerization on stem cells embedded in hydrogels, *Biomaterials*, 2009, **30**(3), 344–353, DOI: 10.1016/j.biomaterials.2008.09.037.

14 S. J. Bryant, C. R. Nuttelman and K. S. Anseth, Cytocompatibility of UV and visible light photoinitiating systems on cultured NIH/3T3 fibroblasts in vitro, *J. Biomater. Sci., Polym. Ed.*, 2000, **11**(5), 439–457, DOI: 10.1163/156856200743805.

15 C. G. Williams, A. N. Malik, T. K. Kim, P. N. Manson and J. H. Elisseeff, Variable cytocompatibility of six cell lines with photoinitiators used for polymerizing hydrogels and cell encapsulation, *Biomaterials*, 2005, **26**(11), 1211–1218, DOI: 10.1016/j.biomaterials.2004.04.024.

16 A. K. Nguyen, P. L. Goering, R. K. Elespuru, S. Sarkar Das and R. J. Narayan, The Photoinitiator Lithium Phenyl (2,4,6-Trimethylbenzoyl) Phosphinate with Exposure to 405 nm Light Is Cytotoxic to Mammalian Cells but Not Mutagenic in Bacterial Reverse Mutation Assays, *Polymers*, 2020, **12**(7), 1489.

17 K. S. Anseth, C. M. Wang and C. N. Bowman, Reaction behaviour and kinetic constants for photopolymerizations of multi(meth)acrylate monomers, *Polymer*, 1994, **35**(15), 3243–3250, DOI: 10.1016/0032-3861(94)90129-5.

18 K. Miyazaki and T. Horibe, Polymerization of multifunctional methacrylates and acrylates, *J. Biomed. Mater. Res.*, 1988, **22**(11), 1011–1022, DOI: 10.1002/jbm.820221105, (acccessed 2024/03/21).

19 P. Martens and K. S. Anseth, Characterization of hydrogels formed from acrylate modified poly(vinyl alcohol) macromers, *Polymer*, 2000, **41**(21), 7715–7722, DOI: 10.1016/S0032-3861(00)00123-3.

20 B. D. Fairbanks, L. J. Macdougall, S. Mavila, J. Sinha, B. E. Kirkpatrick, K. S. Anseth and C. N. Bowman, Photoclick Chemistry: A Bright Idea, *Chem. Rev.*, 2021, **121**(12), 6915–6990, DOI: 10.1021/acs.chemrev.0c01212.

21 M. W. Tibbitt, A. M. Kloxin, L. A. Sawicki and K. S. Anseth, Mechanical Properties and Degradation of Chain and Step-Polymerized Photodegradable Hydrogels, *Macromolecules*, 2013, **46**(7), 2785–2792, DOI: 10.1021/ma302522x.

22 O. Chaudhuri, L. Gu, D. Klumpers, M. Darnell, S. A. Bencherif, J. C. Weaver, N. Huebsch, H.-p. Lee, E. Lippens, G. N. Duda, *et al.*, Hydrogels with tunable stress relaxation regulate stem cell fate and activity, *Nat. Mater.*, 2016, **15**(3), 326–334, DOI: 10.1038/nmat4489.

23 S. Tang, H. Ma, H.-C. Tu, H.-R. Wang, P.-C. Lin and K. S. Anseth, Adaptable Fast Relaxing Boronate-Based Hydrogels for Probing Cell–Matrix Interactions, *Adv. Sci.*, 2018, **5**(9), 1800638, DOI: 10.1002/advs.201800638, (acccessed 2024/03/21).

24 A. Elosegui-Artola, A. Gupta, A. J. Najibi, B. R. Seo, R. Garry, C. M. Tringides, I. de Lázaro, M. Darnell, W. Gu, Q. Zhou, *et al.*, Matrix viscoelasticity controls spatiotemporal tissue organization, *Nat. Mater.*, 2023, **22**(1), 117–127, DOI: 10.1038/s41563-022-01400-4.

25 O. Chaudhuri, Viscoelastic hydrogels for 3D cell culture, *Biomater. Sci.*, 2017, **5**(8), 1480–1490, DOI: 10.1039/C7BM00261K.

26 P. Klán, T. Šolomek, C. G. Bochet, A. Blanc, R. Givens, M. Rubina, V. Popik, A. Kostikov and J. Wirz, Photoremovable Protecting Groups in Chemistry and Biology: Reaction Mechanisms and Efficacy, *Chem. Rev.*, 2013, **113**(1), 119–191, DOI: 10.1021/cr300177k.

27 T. Liu, B. Bao, Y. Li, Q. Lin and L. Zhu, Photo-responsive polymers based on o-Nitrobenzyl derivatives: from structural design to applications, *Prog. Polym. Sci.*, 2023, **146**, 101741, DOI: 10.1016/j.progpolymsci.2023.101741.

28 M. A. Azagarsamy, I. A. Marozas, S. Spaans and K. S. Anseth, Photoregulated Hydrazone-Based Hydrogel Formation for Biochemically Patterning 3D Cellular Microenvironments, *ACS Macro Lett.*, 2016, **5**(1), 19–23, DOI: **10.1021/acsmacrolett.5b00682**.

29 C. Wang, Y. Liu, C. Bao, Y. Xue, Y. Zhou, D. Zhang, Q. Lin and L. Zhu, Phototriggered labeling and crosslinking by 2-nitrobenzyl alcohol derivatives with amine selectivity, *Chem. Commun.*, 2020, **56**(15), 2264–2267, DOI: **10.1039/C9CC09449K**.

30 Y. Hua, H. Xia, L. Jia, J. Zhao, D. Zhao, X. Yan, Y. Zhang, S. Tang, G. Zhou, L. Zhu, *et al.*, Ultrafast, tough, and adhesive hydrogel based on hybrid photocrosslinking for articular cartilage repair in water-filled arthroscopy, *Sci. Adv.*, 2021, **7**(35), eabg0628, DOI: **10.1126/sciadv.abg0628**, (acccessed 2024/03/21).

31 Y. Hong, F. Zhou, Y. Hua, X. Zhang, C. Ni, D. Pan, Y. Zhang, D. Jiang, L. Yang, Q. Lin, *et al.*, A strongly adhesive hemostatic hydrogel for the repair of arterial and heart bleeds, *Nat. Commun.*, 2019, **10**(1), 2060, DOI: **10.1038/s41467-019-10004-7**.

32 Y. Yang, J. Zhang, Z. Liu, Q. Lin, X. Liu, C. Bao, Y. Wang and L. Zhu, Tissue-Integratable and Biocompatible Photogelation by the Imine Crosslinking Reaction, *Adv. Mater.*, 2016, **28**(14), 2724–2730, DOI: **10.1002/adma.201505336**, (acccessed 2024/03/21).

33 A.-D. Guo, D. Wei, H.-J. Nie, H. Hu, C. Peng, S.-T. Li, K.-N. Yan, B.-S. Zhou, L. Feng, C. Fang, *et al.*, Light-induced primary amines and o-nitrobenzyl alcohols cyclization as a versatile photoclick reaction for modular conjugation, *Nat. Commun.*, 2020, **11**(1), 5472, DOI: **10.1038/s41467-020-19274-y**.

34 R. Rizzo, D. Rütsche, H. Liu, P. Chansoria, A. Wang, A. Hasenauer and M. Zenobi-Wong, Multiscale Hybrid Fabrication: Volumetric Printing Meets Two-Photon Ablation, *Adv. Mater. Technol.*, 2023, **8**(11), 2201871, DOI: **10.1002/admt.202201871**, (acccessed 2024/03/14).

35 L. Oxburgh, T. J. Carroll, O. Cleaver, D. R. Gossett, D. K. Hoshizaki, J. A. Hubbell, B. D. Humphreys, S. Jain, J. Jensen, D. L. Kaplan, *et al.*, (Re)Building a Kidney, *J. Am. Soc. Nephrol.*, 2017, **28**(5), 1370–1378.

36 R. A. Wimmer, A. Leopoldi, M. Aichinger, D. Kerjaschki and J. M. Penninger, Generation of blood vessel organoids from human pluripotent stem cells, *Nat. Protoc.*, 2019, **14**(11), 3082–3100, DOI: **10.1038/s41596-019-0213-z**.

37 R. Zhou, Y. Hua, L. Yang, B. Bao, Q. Lin and L. Zhu, Reinforced hydrogel network building by a rapid dual-photo-coupling reaction for 3D printing, *Chem. Commun.*, 2023, **59**(14), 1963–1966, DOI: **10.1039/D2CC05677A**.

38 S. Kazanis and R. A. McClelland, Electrophilic intermediate in the reaction of glutathione and nitroso arenes, *J. Am. Chem. Soc.*, 1992, **114**(8), 3052–3059, DOI: **10.1021/ja00034a043**.

39 P. Eyer, Reactions of nitrosobenzene with reduced glutathione, *Chem.-Biol. Interact.*, 1979, **24**(2), 227–239, DOI: **10.1016/0009-2797(79)90011-5**.

40 D. T. Hess, A. Matsumoto, S.-O. Kim, H. E. Marshall and J. S. Stamler, Protein S-nitrosylation: purview and parameters, *Nat. Rev. Mol. Cell Biol.*, 2005, **6**(2), 150–166, DOI: **10.1038/nrm1569**.

41 V. Fernando, X. Zheng, Y. Walia, V. Sharma, J. Letson and S. Furuta, S-Nitrosylation: An Emerging Paradigm of Redox Signaling, *Antioxidants*, 2019, **8**(9), 404.

42 J. S. Zhu, N. Kraemer, M. E. Shatskikh, C. J. Li, J.-H. Son, M. J. Haddadin, D. J. Tantillo and M. J. Kurth, N–N Bond Formation between Primary Amines and Nitrosos: Direct Synthesis of 2-Substituted Indazolones with Mechanistic Insights, *Org. Lett.*, 2018, **20**(16), 4736–4739, DOI: **10.1021/acs.orglett.8b01655**.

43 W. H. Stockmayer, Theory of Molecular Size Distribution and Gel Formation in Branched Polymers II, General Cross Linking, *J. Chem. Phys.*, 1944, **12**(4), 125–131, DOI: **10.1063/1.1723922**, (acccessed 6/19/2024).

44 P. J. Flory, Molecular Size Distribution in Three Dimensional Polymers, I. Gelation1, *J. Am. Chem. Soc.*, 1941, **63**(11), 3083–3090, DOI: **10.1021/ja01856a061**.

45 R. G. Allen and M. Tresini, Oxidative stress and gene regulation, *Free Radicals Biol. Med.*, 2000, **28**(3), 463–499, DOI: **10.1016/S0891-5849(99)00242-7**.

46 A. Chrisnandy, D. Blondel, S. Rezakhani, N. Broguiere and M. P. Lutolf, Synthetic dynamic hydrogels promote degradation-independent in vitro organogenesis, *Nat. Mater.*, 2022, **21**(4), 479–487, DOI: **10.1038/s41563-021-01136-7**.

47 J. G. Roth, M. S. Huang, R. S. Navarro, J. T. Akram, B. L. LeSavage and S. C. Heilshorn, Tunable hydrogel viscoelasticity modulates human neural maturation, *Sci. Adv.*, 2023, **9**(42), eadh8313, DOI: **10.1126/sciadv.adh8313**, (acccessed 2024/03/21).

48 A. N. Borelli, M. W. Young, B. E. Kirkpatrick, M. W. Jaeschke, S. Mellett, S. Porter, M. R. Blatchley, V. V. Rao, B. V. Sridhar and K. S. Anseth, Stress Relaxation and Composition of Hydrazone-Crosslinked Hybrid Biopolymer-Synthetic Hydrogels Determine Spreading and Secretory Properties of MSCs, *Adv. Healthcare Mater.*, 2022, **11**(14), 2200393, DOI: **10.1002/adhm.202200393**, (acccessed 2024/03/21).

49 M. Xie, L. Lian, X. Mu, Z. Luo, C. E. Garciamendez-Mijares, Z. Zhang, A. López, J. Manríquez, X. Kuang, J. Wu, *et al.*, Volumetric additive manufacturing of pristine silk-based (bio)inks, *Nat. Commun.*, 2023, **14**(1), 210, DOI: **10.1038/s41467-023-35807-7**.

50 L. Lian, M. Xie, Z. Luo, Z. Zhang, S. Maharjan, X. Mu, C. E. Garciamendez-Mijares, X. Kuang, J. K. Sahoo, G. Tang, *et al.*, Rapid Volumetric Bioprinting of Decellularized Extracellular Matrix Bioinks, *Adv. Mater.*, 2024, 2304846, DOI: **10.1002/adma.202304846**, (acccessed 2024/03/21).

51 A. Gulzar, E. Yıldız, H. N. Kaleli, M. A. Nazeer, N. Zibandeh, A. N. Malik, A. Y. Taş, I. Lazoğlu, A. Şahin and S. Kizilel, Ruthenium-induced corneal collagen cross-linking under visible light, *Acta Biomater.*, 2022, **147**, 198–208, DOI: **10.1016/j.actbio.2022.05.040**.

